# A Direct AC–DC and DC–DC Cross-Source Energy Harvesting Circuit with Analog Iterating-Based MPPT Technique with 72.5% Conversion Efficiency and 94.6% Tracking Efficiency

Shin-Hao Chen, Tzu-Chi Huang, *Student Member, IEEE*, Shao Siang Ng, Kuei-Liang Lin, Ming-Jhe Du, Yu-Chai Kang, Ke-Horng Chen, *Senior Member, IEEE*, Chin-Long Wey, Ying-Hsi Lin, Chao-Cheng Lee, Jian-Ru Lin, and Tsung-Yen Tsai

***Abstract*—The proposed cross-source energy (CSE) harvesting system accepts universal energy sources, including the ac and dc sources. The buck–boost conversion of CSE automatically converts ac or dc input into dc output without being limited by the type of universal energy source. The CSE technique simultaneously supplies the regulated output for the system loading and the battery charging output. A test chip fabricated in the VIS Bipolar, CMOS, and DMOS (BCD) process can optimally derive harvest energy with 72.5% power efficiency when one solar input source is used. A backup converter is designed to complement the CSE technique to guarantee the regulation of output voltage. The proposed analog iterating-based (AIB) maximum power point tracking (MPPT) technique achieves 94.6% tracking efficiency without complex data calculation and storage, which are better results compared with those of previous research.**

***Index Terms*—Analog iterating-based (AIB) maximum power point tracking (MPPT) technique, cross-source energy (CSE) harvesting system, universal energy sources.**

## I. Introduction

ENERGY harvesting techniques have been widely discussed on wireless sensor networks or portable applications [1]–[4]. The most commonly discussed applications include wireless sensor nodes (WSNs) for health care, embedded or implanted sensor nodes for medical applications, tire pressure monitoring in automobiles, battery recharging of long-sustainability systems, security or guard systems in housekeeping, and environment change monitor systems. In particular, the Internet of Things (IoT) requires energy-harvesting techniques to obtain sufficient energy for extended battery usage time.

As depicted in Fig. 1, energy sources can be divided into two basic types: direct current (dc) and alternating current (ac) energy sources. DC energy sources include thermal energy and solar energy. By contrast, there are many types of ac energy sources, such as electromagnetic radiation, wind power, RF power, and kinetic energy [5]–[14]. In this paper, the input power range of the proposed cross-source energy (CSE) harvesting circuit is 200 $\mu$W to 50 mW. Input voltage can range from 0.06 to 5 V. According to Fig. 1, the energy sources that can be utilized are solar cell, wind power generator, magnetic coil, and piezoelectric kinetic energy. However, the output power of the harvested RF and thermal energy is lower than the required energy of some complex systems. Moreover, the energy supply of a harvesting source may not satisfy the high-power consumption of an application. Battery capacity and power delivery path require proper settings to maintain proper function.

Batteries are the most commonly used power source in conventional portable electronics. Considering the use of an energy-harvesting system, the overall performance needs to outperform a battery solution in energy density, power density, and/or cost. Typically, the niche for energy harvesting is in long-lived applications where energy density is critical and the location of the devices may not be reachable [7].

To overcome the disadvantages of both energy-harvested and battery-supplied systems, a hybrid mode power supply system is recommended. Recharging a battery is preferred when using a harvested-energy system. The battery supplies high power (up to several mWs) during a short period of time (as the receiving, transmitting, and polling mode), whereas the energy harvester charges the battery with a trickle current during the remainder of the time. Fig. 2 shows the system diagram of a conventional cascaded harvesting system. AC–DC and DC–DC converter stages deal with the input source to generate charging current to the storage device. The DC–DC converter stage regulates the system. This structure conforms to the preferred scenario, and it is commonly used in many applications. However, the

Manuscript received February 1, 2015; accepted September 29, 2015. Date of publication October 12, 2015; date of current version March 2, 2016. This work was supported by the National Science Council, Taiwan, under Grant MST 103-2622-E-009-010-CC2, Grant MST 103-2923-E-009-005-MY3, Grant MST 103-2221-E-009-074-MY3, and Grant MST 103-2220-E-009-022. Recommended for publication by Associate Editor Carlos Alberto Canesin.

S.-H. Chen, K.-L. Lin, M.-J. Du, K.-H. Chen, and C.-L. Wey are with the Institute of Electrical Control Engineering, National Chiao Tung University, Hsinchu 30010, Taiwan (e-mail: ff80628@hotmail.com; lin6448@yahoo.com.tw; 3379416@gmail.com).

T.-C. Huang was with the Institute of Electrical Control Engineering, National Chiao Tung University, Hsinchu, Taiwan. He is now with MediaTek Inc., Hsinchu 30010, Taiwan (e-mail: bluecolin07@hotmail.com).

S. S. Ng is with the Institute of Electrical Control Engineering, National Chiao Tung University, Hsinchu, Taiwan, and also with MediaTek Inc., Hsinchu 30010, Taiwan (e-mail: shao0804@gmail.com).

Y.-C. Kang is with the Institute of Electrical Control Engineering, National Chiao Tung University, Hsinchu, Taiwan, and also with Taiwan Semiconductor Manufacturing Corp. (TSMC), Hsinchu 30010, Taiwan (e-mail: quarkskang@gmail.com).

Y.-H. Lin, C.-C. Lee, J.-R. Lin, and T.-Y. Tsai Realtek Semiconductor Corp., Hsinchu 30010, Taiwan.

Color versions of one or more of the figures in this paper are available online at http://ieeexplore.ieee.org.

Digital Object Identifier 10.1109/TPEL.2015.2489922

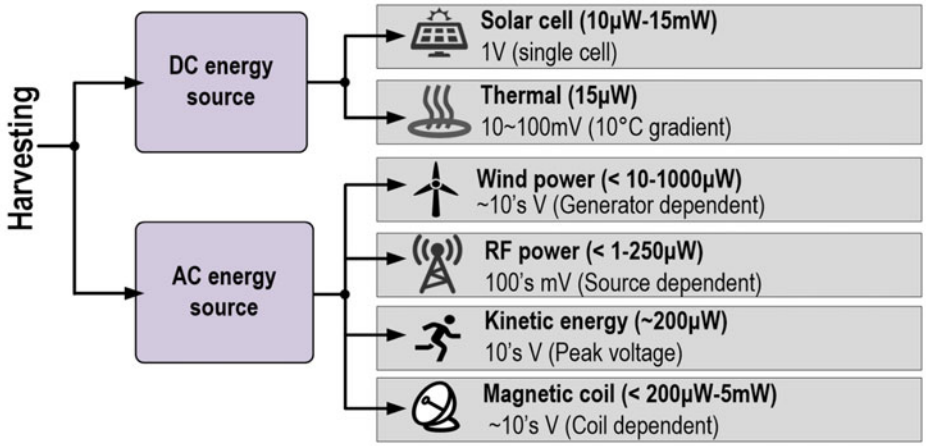


Fig. 1. Available energy in environment.

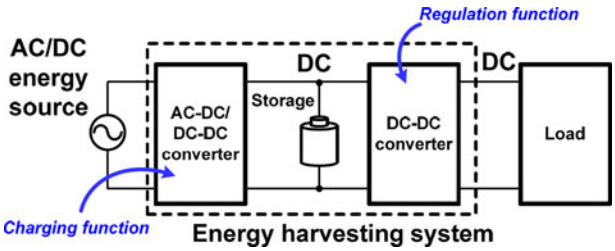


Fig. 2. System diagram of a conventional serial structure harvesting system.

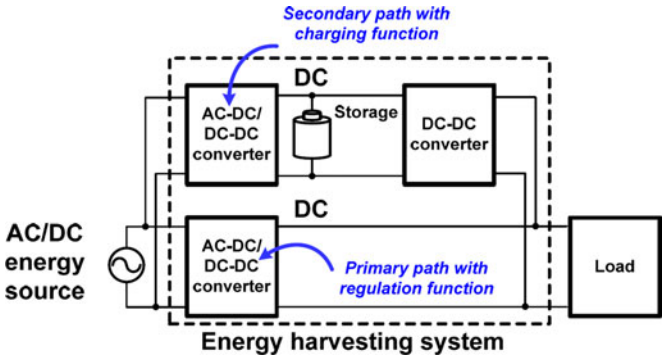


Fig. 3. System diagram of a parallel structure harvesting system.

conversion of the input energy uses the two-step approach, which results in low efficiency. To further optimize conversion efficiency and reduce energy loss, the additional conversion loss induced by two-stage structure can be lowered if the energy is directly transferred to the output load.

The system diagram of a parallel structure harvesting system is shown in Fig. 3. The parallel structure can improve conversion efficiency and maintain charging function. The parallel structure takes a primary path to directly convert energy to the load using a single conversion stage to avoid additional conversion power loss. The secondary path transfers redundant energy to the storage device during charging when the energy source generates more energy than the required load. A DC–DC converter is placed after the battery to supply the primary path once the energy source becomes insufficient. This structure brings more design challenges compared with the conventional cascaded structure. First, the primary path of an AC–DC/DC–DC converter must regulate output voltage. Second, an energy distribution scheme is required to accurately allot input energy to primary and secondary paths because the two paths share the same energy source. Finally, the overhead cost and area caused by extra circuits must be considered.

Many harvesting circuits are similar to conventional power converters. However, primary differences exist between energy-harvesting circuit designs and conventional DC–DC or AC–DC converter designs. These differences are listed as follows:

1) energy quantity from the source is limited; hence, the loading condition of the system has to meet the characteristics of the energy-harvesting source;
2) the energy source is not a fixed voltage or current source; load or environment also varies;
3) input voltage may be very low or vary over a wide range;
4) operation voltage and current have to be defined according to the MPP.

This paper is organized as follows. The proposed CSE harvesting system and analog iterating-based (AIB) maximum power point tracking (MPPT) are shown in Sections II and III, respectively. Section IV discusses the experimental results. Finally, conclusions are presented in Section V.

## II. Proposed CSE Harvesting System

### A. AC Source Energy Harvesting Circuits

In traditional designs, an energy-harvesting circuit with an ac source has several targets. The ac input must be rectified to the dc value; otherwise, energy is hardly used or stored. The magnitude of an ac source in the harvesting system varies according to environmental conditions. Thus, setting a voltage limit for some ac applications is required to protect the circuit from overvoltage damage. A two-stage approach, as depicted in Fig. 2, is the mainstream in ac source harvesting, and this has been presented in previous literature. According to the input voltage and current range, the AC–DC structure is required to convert the input voltage to a proper voltage level for back-end usage. Fig. 4 shows the summary and function comparison of the harvesting structures. The rectifiers and converters are listed from

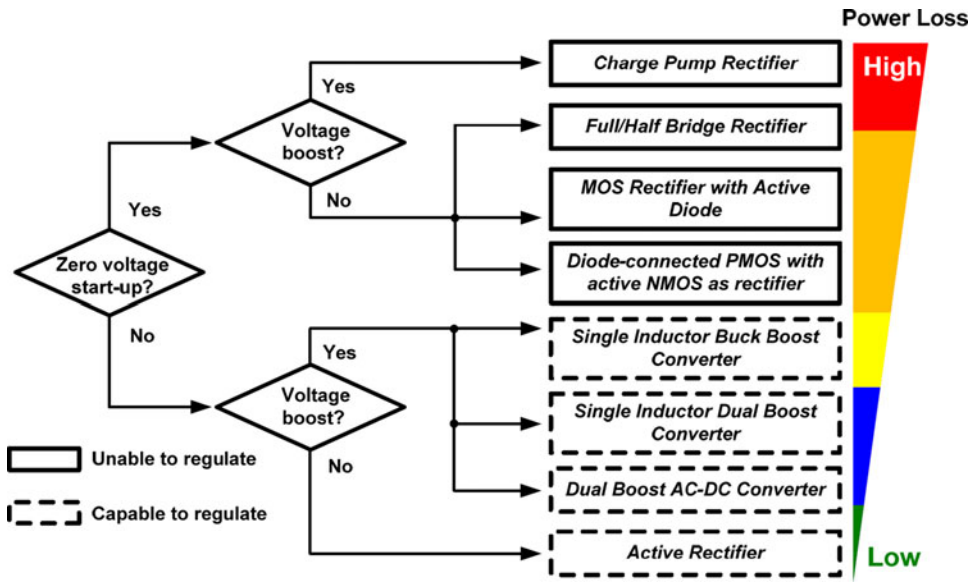


Fig. 4. Function selection and characteristics of different AC–DC structures.

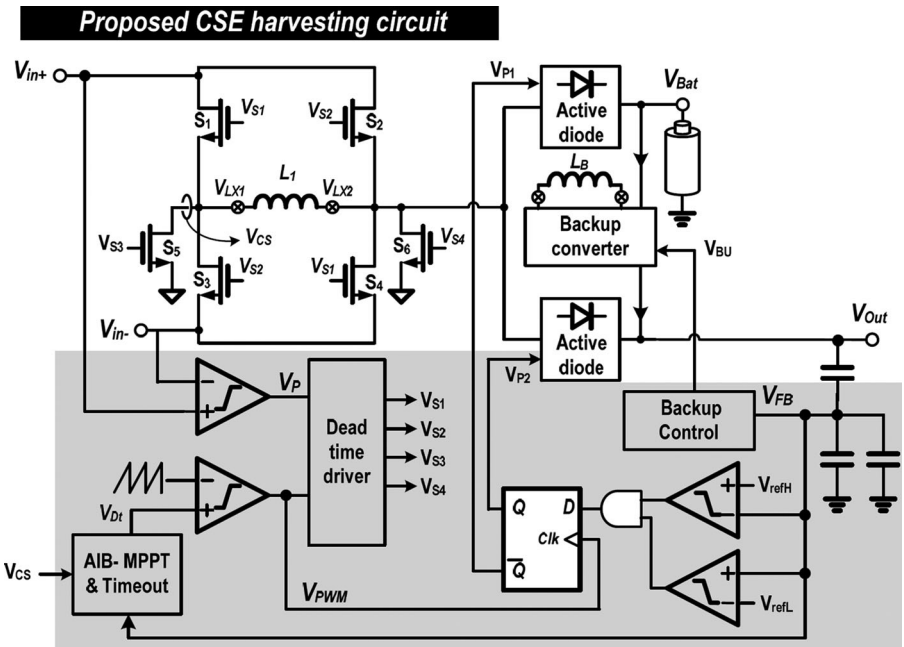


Fig. 5. Proposed harvesting circuit and power deliver diagram.

high to low power loss and classified according to the different function requirements. One diode has the forward voltage drop $V_D$ (approximately 0.7 V) between two terminals, whereas the voltage drop of one MOSFET is significantly smaller than $V_D$ and inversely proportional to its aspect ratio. The active rectifier structure achieves minimum power loss compared with other AC–DC structures. Harvesting efficiency is defined as output power $P_O$ divided by available input power $P_{\rm IN}$ [15]. Power loss $P_{\rm LOSS}$ in a power delivery path determines the overall efficiency $\eta_H$, as illustrated

$$\eta_H = \frac{P_O}{P_{\rm IN}} = \frac{P_{\rm IN} - P_{\rm LOSS}}{P_{\rm IN}} = \frac{P_{\rm IN} - P_C - P_{\rm SW}}{P_{\rm IN}} \quad (1)$$

where $P_C = i^2_{L,\rm RMS} \cdot R_S \propto i^2_{\rm IN,AVG}$.

Conduction loss $P_C$ is low because resistance $R_S$ of each switch is slight. Moreover, $P_C$ decreases quadratically with input power $P_{\rm IN}$. Hence, a simple instruction is provided to determine the structure and design of the harvesting circuit.

### *B. DC Source Energy-Harvesting Circuits*

In energy harvesting, the number of ac sources is higher than that of dc sources. The most widely discussed dc harvesting sources include thermal electric generator and solar cell. The dc harvesting circuit aims to convert input voltage to a proper and regulated voltage level for battery charging or system supply. The energy conversion of dc source harvesting circuits is simpler than that of ac source harvesting circuits because it is similar

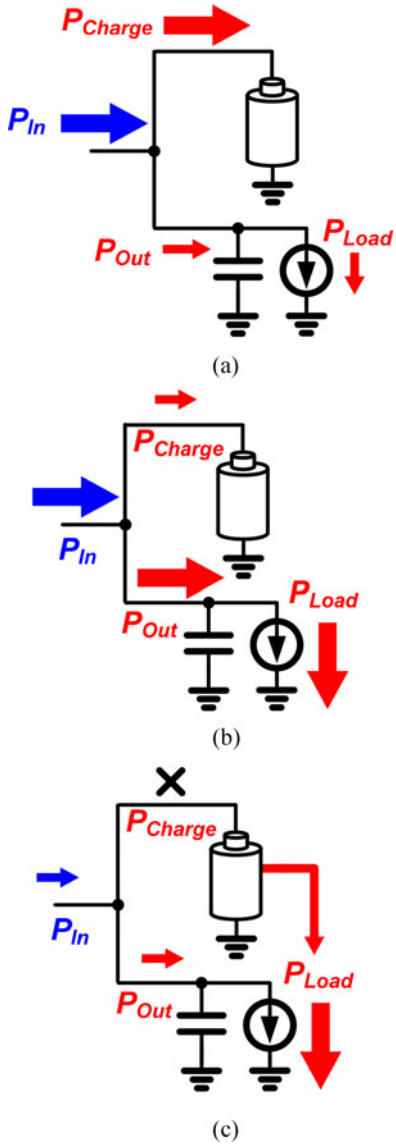


Fig. 6. Energy distribution priority. (a) Input energy is used to charge the battery when loading is low. (b) Input energy is used to supply the loading when loading increases. (c) Input energy mainly supplies the loading and disconnects from the battery when input energy decreases.

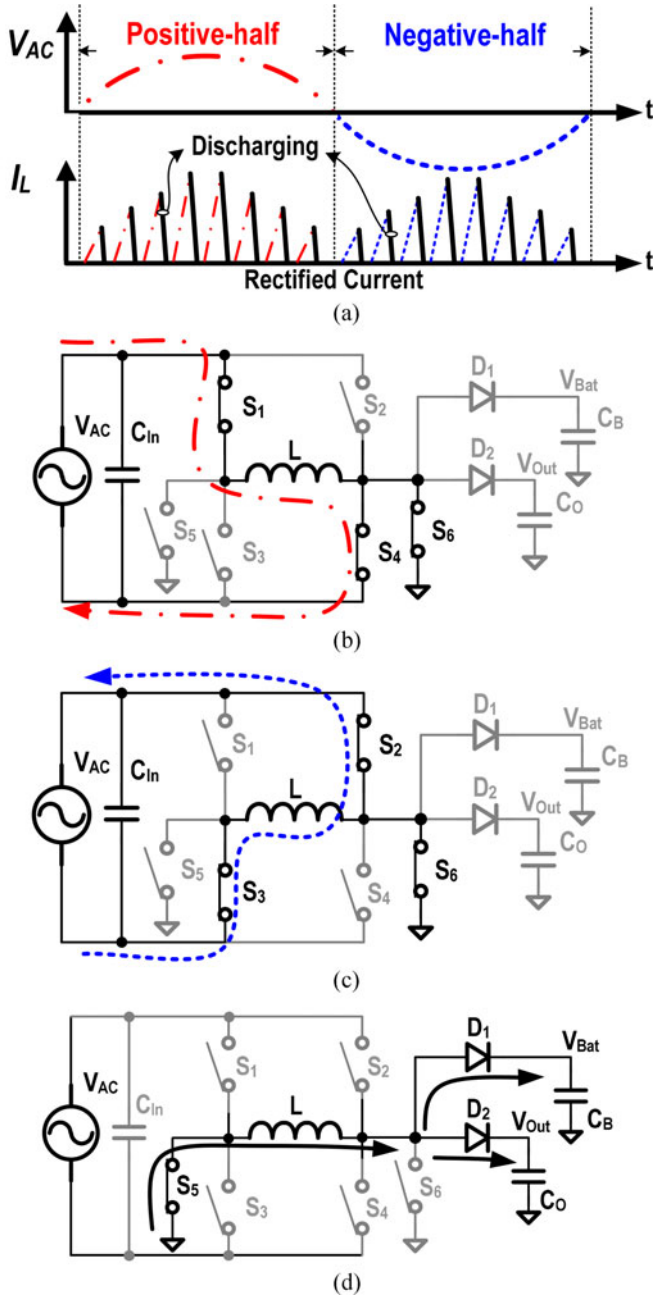


Fig. 7. AC input current paths. (a) Waveforms. (b) Positive-half charging path. (c) Negative-half charging path. (d) Discharging path.

to conventional DC–DC converters. DC–DC harvesting circuits can use DC–DC converters to perform voltage regulation in the system diagram shown in Figs. 2 and 3.

DC–DC harvesting circuits and conventional DC–DC converters have the same design goals. However, the quiescent power is a more important issue in harvesting circuits than in conventional DC–DC converters. DC–DC converters may require reference voltage or bias current that some subcircuits can provide to support the DC–DC converter regularly. Some subcircuits such as bandgap voltage reference, comparators, and amplifiers consume a considerable amount of power. Power loss may reach up to hundreds of $\mu$Ws. If DC–DC converters convert large output power or require fast transient response, high power consumption caused by the controller is necessary. However, for low-input power applications, such as harvesting circuits, the cost of power consumption may not be affordable. Moreover, the input power achieved may be less than the input power that can be possibly derived. Thus, one of the challenges of DC–DC harvesting circuits is designing an ultralow power operation scheme and the corresponding low-power control circuit.

In previous designs, each harvesting circuit is designed for ac or dc sources. Although custom-made harvesting circuits achieve better efficiency or have a smaller chip area, these circuits have many disadvantages. Developing a custom-made harvesting circuit for any energy source is problematic and not cost-effective. The difference between each energy source is significant; hence, the output power range, output current range, and output voltage stability are difficult to control. Moreover,

the functions of these circuits are limited to a narrow input range or can only receive a specific ac frequency. Therefore, a harvesting circuit that is compatible with a global energy source is the perfect solution. In a WSN design, the circuit with a wide input range can simultaneously harvest all energy sources, such as solar cell (dc source), wind power (ac source), and RF power (ac source with different frequencies). As a result, the received energy as well as the energy collecting speed can be higher than those of other single-sourced harvesting structures.

The difficulties encountered when one harvesting circuit is applied to universal energy sources, including ac and dc sources, should be addressed. First, the power stage should be used if ac or dc input is received. Low power loss in conversion is a demand. Large input voltage range forces the harvesting circuit to be capable of up or down conversion of the input voltage to the regulated output voltage. Consequently, an active rectifier becomes the suitable option. By synchronously controlling the four power MOSFETs, wide input range and AC–DC or DC–DC converter can be achieved simultaneously. Second, MPPT, which increases harvesting power, is needed. However, the MPPT method must be applied to ac and dc sources at the same time [2], [4]–[6]. Conventional perturb and observe (P&O) method [4]–[6] samples power information periodically. Comparison of the power information of the two continuous samples indicates that the controller adjusts the operation duty or oscillating frequency to maximize input harvesting power [1]–[6]. However, direct ac MPPT must set a sampling period because the operating frequency varies with different sources. The frequency of ac sources that varies from 2.5 Hz to 1 kHz makes it difficult to derive power information without any complex data calculation and storage [1]. Although the ac input source have been used [1], [3], the proposed MPPT has been shown to work only in rectifying dc input voltage instead of directly connecting to an ac source. Conflicting design demand has been observed in previous studies. To overcome the difficulties stated earlier, the proposed CSE harvesting system in Fig. 5 for both ac and dc energy sources should have a direct ac and dc MPPT scheme capable of attaining high efficiency. The schematic diagram in Fig. 5 is described in detail in the succeeding part.

### C. Proposed CSE Harvesting Circuits

The proposed CSE harvesting circuit provides dual outputs, as shown in Fig. 6. One regulated output $V_{\rm Out}$ can supply system loading, and the other output can charge battery $V_{\rm Bat}$. For the input energy source, regulated $V_{\rm Out}$ has higher priority than battery $V_{\rm Bat}$ to maintain the stable operation of the system. The battery can be charged if the input energy is larger than the system loading requirement, as shown in Fig. 6(a) and (b). Both $P_{\rm Charge}$ and $P_{\rm Out}$ can be delivered. The MPPT control monitors the harvesting energy source at its maximum level; thus, an additional battery works as a buffer to store or provide energy if loading at $V_{\rm Out}$ cannot be completely provided by the input energy. As illustrated in Fig. 5, the backup converter connected between the battery and $V_{\rm Out}$ ensures the regulation at $V_{\rm Out}$ if input harvesting energy source is not sufficient, as shown in Fig. 6(c). The battery cannot be charged by $P_{\rm Charge}$ and

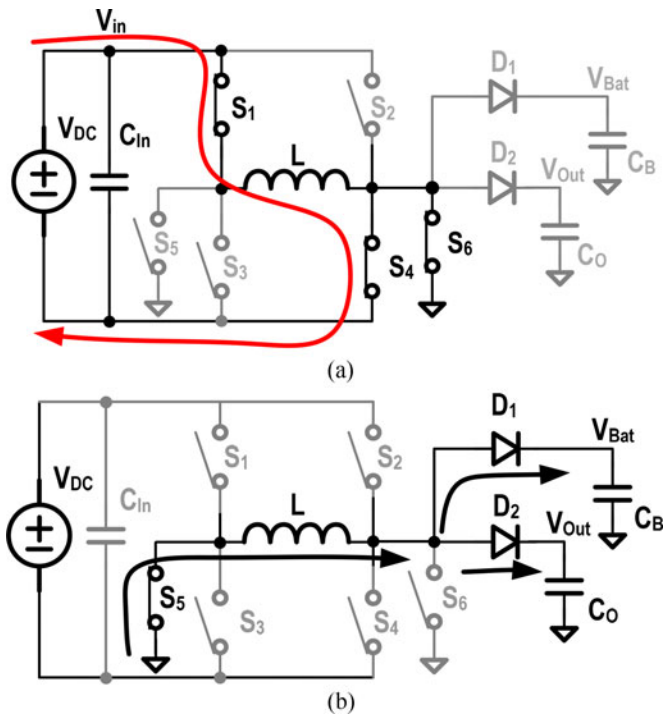


Fig. 8. DC input current paths. (a) DC charging path. (b) Discharging path.

$P_{\rm Load}$ needs to drain current from the battery. In the feedback loop, $V_{{\rm ref}H}$ regulates $V_{\rm Out}$. Furthermore, two active diodes that determine the power delivery path are used to avoid power loss caused by reverse current where $V_{{\rm ref}L}$ is set for the correct operation of the two active diodes. When an active diode is used in a converter design, no reverse power is allowed to flow back to the converter because of its diode-like characteristic.

To accommodate the wide input voltage range from different harvesting sources, the CSE power stage is designed as a buck–boost configuration that is composed of six power MOSFETs. A comparator is connected to $V_{\rm in}+ {\rm and} V_{\rm in}-$ to recognize the polarity of the input source. The AIB-MPPT circuit generates duty control signal $V_{\rm Dt}$ to the fixed frequency pulsewidth modulation (PWM) controller that can generate gate control signals $V_{S1}$--$V_{S4}$, as shown in Fig. 5.

Figs. 7 and 8 show the AC–DC and DC–DC conversion power delivery paths, respectively. CSE works in a discontinuous conduction mode (DCM). In AC–DC conversion, switches $S_1$ and $S_4$ are turned on to charge the inductor current during a positive half charging path, as shown in Fig. 7(b). By contrast, switches $S_2$ and $S_3$ are turned on to charge the inductor current during a negative half charging path, as illustrated in Fig. 7(c). The inductor discharges energy through the discharging path formed by shorting $S_5$ to the ground, as shown in Fig. 7(d). The negative part of the ac source will be forced to the chip's ground by shorting switch $S_6$. The ground-connected structure releases the harvesting energy produced by engaging negative voltage and reduces the risk of body diode leakage. The rectified inductor current can be always positive. As a result, the harvesting energy source is not necessary an ac or dc source; CSE can harvest any arbitrary type of current source without being limited to periodic

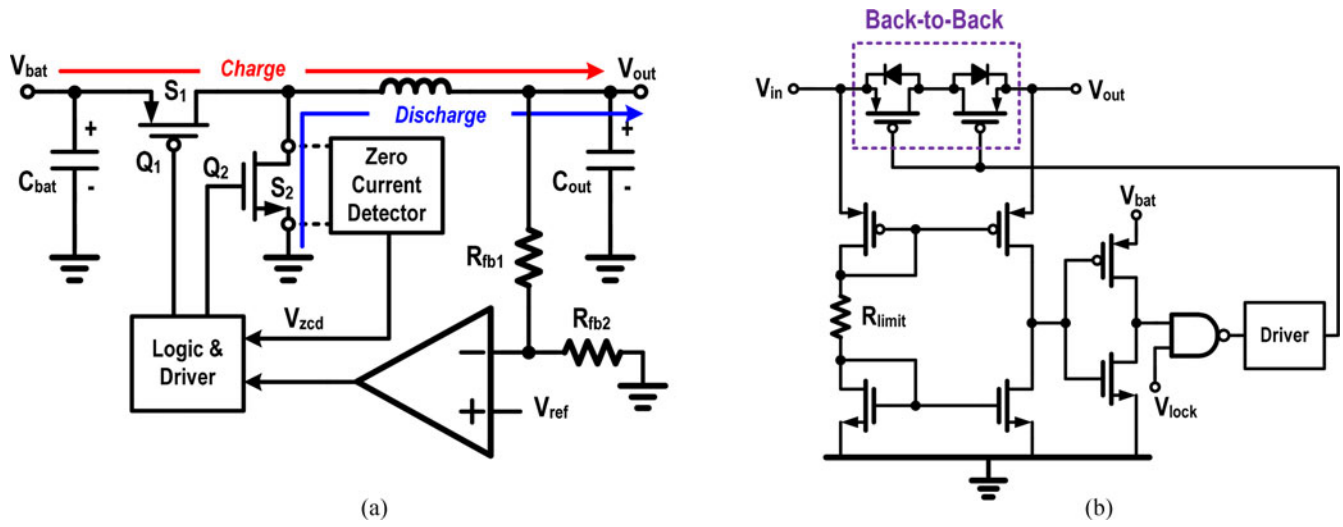


Fig. 9. Circuit implementation of (a) backup converter and (b) active diode.

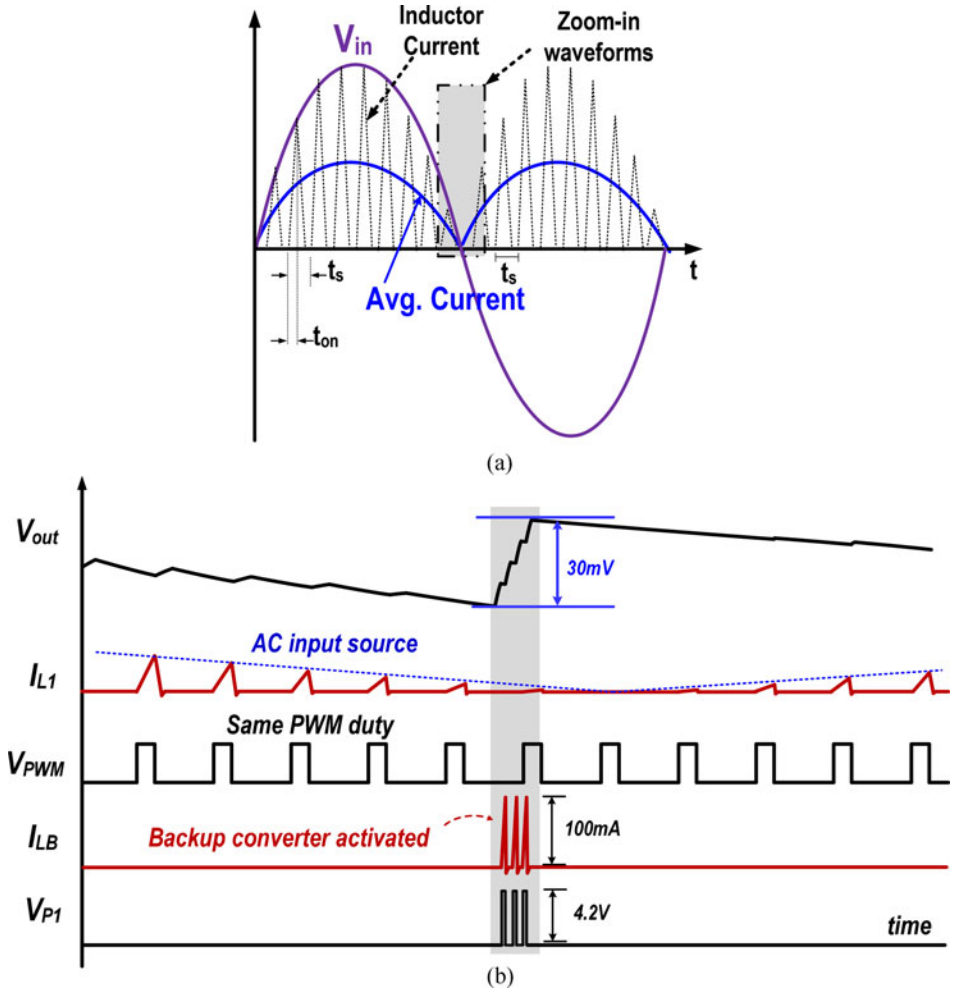


Fig. 10 (a) Waveforms of CSE harvesting circuit. (b) Zoom-in waveforms.

signals. Moreover, in DC–DC mode, switches $S_1$ and $S_4$ are turned on to charge the inductor current, as depicted in Fig. 8(a). Inductor $L$ discharges power by shorting $S_5$ to the ground, as shown in Fig. 8(b). CSE operates simply as a buck–boost converter [5].

Fig. 9(a) shows the circuit implementation of the backup converter. $V_{\mathrm{Bat}}$ is always higher than $V_{\mathrm{Out}}$; hence, the backup converter is a buck converter working in DCM with zero-current-detection (ZCD) circuit for high efficiency. The active diode circuit is depicted in Fig. 9(b) as the comparison between

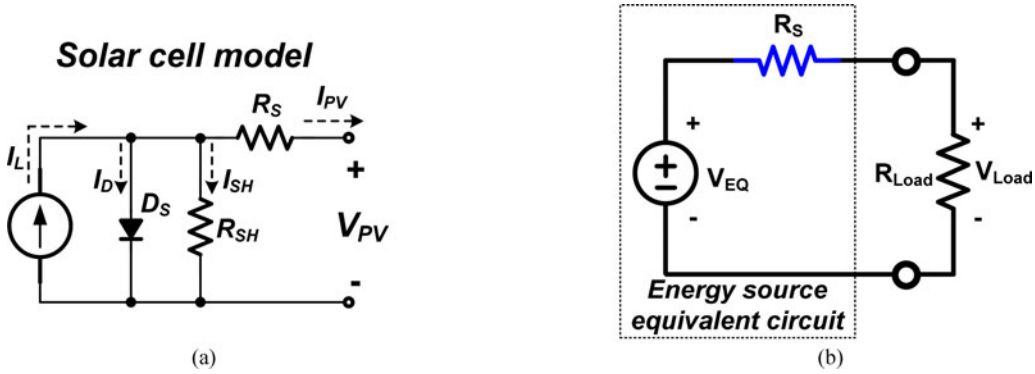


Fig. 11 (a) Modeling of the solar cell and (b) Thevenin equivalent circuit of energy source.

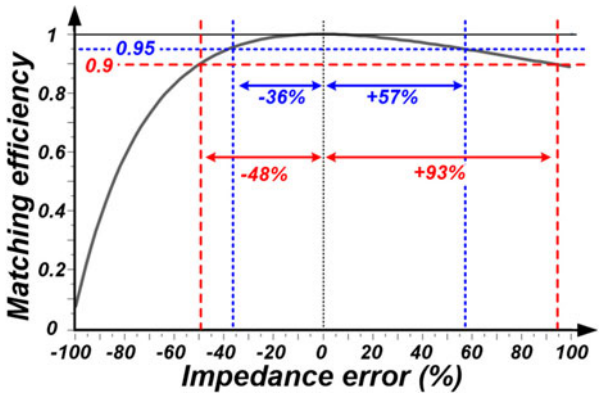


Fig. 12. Matching efficiency versus impedance error.

$V_{\rm in}$ and $V_{\rm out}$ to determine the conduction of the active diode. When $V_{\rm in}$ is larger than $V_{\rm out}$, back-to-back configuration will be conducted. On the contrary, when $V_{\rm in}$ is smaller than $V_{\rm out}$, the back-to-back configuration will be disconnected. Voltage $V_{\rm lock}$ is connected to $V_{P1}$ and $V_{P2}$ to determine the power delivery path in Fig. 5. Resistor $R_{\rm limit}$ can limit the current consumption of the active diode.

Fig. 10(a) shows the waveform of the proposed CSE harvesting circuit operating at a fixed frequency of 10 kHz if the input energy source has an ac frequency of 500 Hz. The zoom-in waveforms of Fig. 10(b) show that once the output voltage is 30 mV below the target voltage due to insufficient harvesting energy source or load current changes in case of light-to-heavy loading current variation, the backup converter will be triggered. $V_{P1}$ has 4.2 V rail-to-rail pulses, and the battery charges back-up inductor $L_B$ to 100 mA current.

## III. Analog Iterating-Based MPPT

Various harvesting sources, such as photovoltaic, thermal electric, vibration, or magnetic coil, have their own electrical and mechanical properties. Output voltage, current, and power of each source are influenced by the loading effect. For each source in a steady state, a specific output voltage and current condition that delivers maximum output power can be derived. The point is selected as MPP, and the equivalent load on the MPP is defined and tracked through the MPPT control [1], [7], [16].

Fig. 11(a) shows the equivalent model of solar cells. First, current $I_L$ generated by solar cells is assumed to be constant in a steady irradiation condition. If the load at output voltage $V_{\rm PV}$ is low, $V_{\rm PV}$ increases, and leakage current on the parasitic diode $D_S$ and resistance $R_{\rm SH}$ is induced. If the load is high, $V_{\rm PV}$ drops. Most of the power is wasted on series resistance $R_S$. Thus, it is important to determine MPP to enable the extraction of maximum power under the same environment condition. Many harvesting systems have proposed useful MPPT circuits to enhance efficiency and derive the maximum output power [1], [7], [12], [17]–[19]. Some issues that need to be considered in a harvesting system with the MPPT function are as follows:

1) the characteristic of energy sources must be determined before using the MPPT method;
2) power consumption of the MPPT circuit is critical for many low-power applications;
3) MPPT control will force the input source attain its maximum output energy;
4) storage device is necessary if the harvesting system intends to have MPPT function;
5) to overcome environmental variations, continuous tracking is necessary.

MPP varies under different environmental conditions. Harvesting circuits need to control the power delivery condition to maintain the operation of the energy-harvesting system at its MPP. The MPPT scheme is a method that tracks input power. If a harvesting system directly provides supply voltage to the load system, the MPPT function disables the harvesting system to regulate the output voltage at the same time; this will occur unless the input power is always the same as the load requirement, which is not possible. Thus, the following general ideas and methods for implementing the MPPT control are introduced.

### A. Impedance Matching

Many harvesting sources have a complex behaviors or models of their internal equivalent circuit. Previous studies [1], [12], [20], [21] have presented many optimized designs for different characteristics of harvesting sources. These designs have outstanding output power performance because of their special operation schemes. However, these circuits can only be applied to specific sources. Impedance matching method, which is the most popular and important approach, is a general purpose

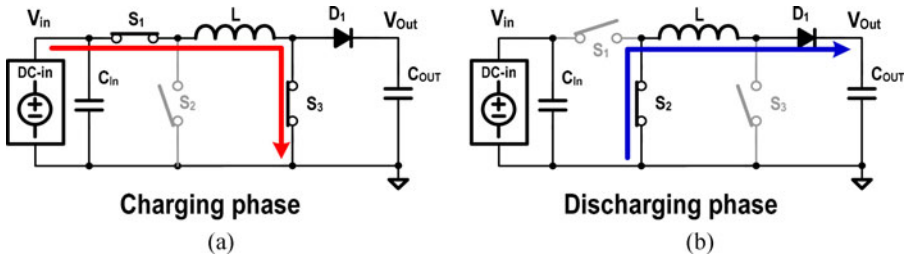


Fig. 13. Buck–boost converter operation in (a) charging and (b) discharging phases.

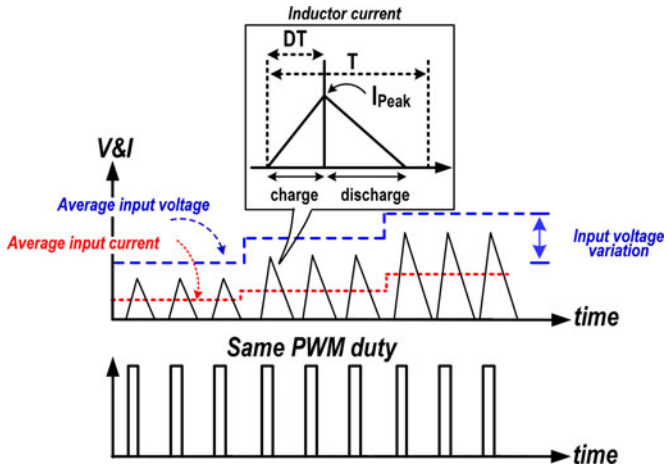


Fig. 14. Inductor current under DCM operation.

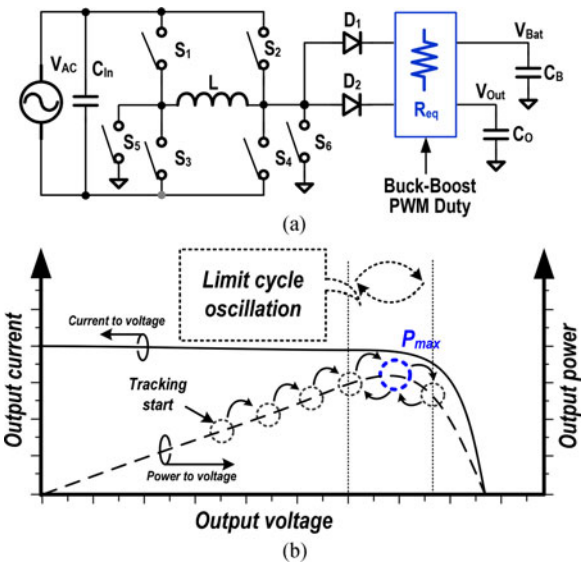


Fig. 15 (a) Using PWM duty to adjust the value of $R_{\rm eq}$. (b) Output power and output current versus output voltage of solar cells if the MPPT is used.

MPPT scheme that can be applied to different sources. Fig. 11(b) shows the Thevenin equivalent circuit of an energy-harvesting source that is modeled as ideal voltage source $V_{\rm EQ}$ with series resistance $R_S$. Generally, all sources can be modeled as Fig. 11(b) with different Thevenin equivalent impedances even if the impedance is not pure resistance and inductance and capacitance are included. However, matching the load impedance

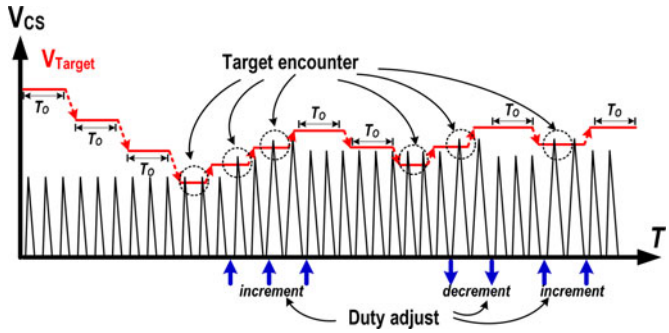


Fig. 16. Target power and the sampled power status iteratively track each other due to the proposed AIB-MPPT.

with inner impedance is still valid and provides tracking instructions when the MPPT is desired.

Power $P_{\rm Load}$ on output loading $R_{\rm Load}$ is shown as follows:

$$P_{\rm Load} = I_{\rm Load}^2 \cdot R_{\rm Load} = \left(\frac{V_{\rm EQ}}{R_S + R_{\rm Load}}\right)^2 \cdot R_{\rm Load}. \quad (2)$$

Impedance matching theory implies that a system achieves maximum power transfer when the loading impedance is equal to the inner impedance. Maximum output power $P_{\rm Load,max}$ is expressed as (3). Matching efficiency $\eta_m$ is defined as the ratio of $P_{\rm Load}$ to $P_{\rm Load,max}$, as shown in (4)

$$P_{\rm Load,max} = \frac{V_{\rm EQ}^2}{4R_{\rm Load}} \quad (3)$$

$$\eta_m = \frac{P_{\rm Load}}{P_{\rm Load,max}} = \frac{4}{1 + (2R_S/R_{\rm Load}) + (R_S/R_{\rm Load})^2}. \quad (4)$$

Fig. 12 shows the matching efficiency under different impedance errors. Impedance error represents the mismatch percentage as compared with the inner impedance of the harvesting source. When the load impedance is perfectly matched with the inner impedance, the error percentage is zero and the matching efficiency is consistent. If 90% matching efficiency is desired, the endurable load impedance error ranges from $-48\%$ to $+93\%$. A wide endurable range indicates that even when a large impedance error percentage occurs, the output power remains very close to the MPP.

### B. Resistor Emulation

Regardless of type, whether switching or linear power converters, an equivalent resistance of the converter can be obtained

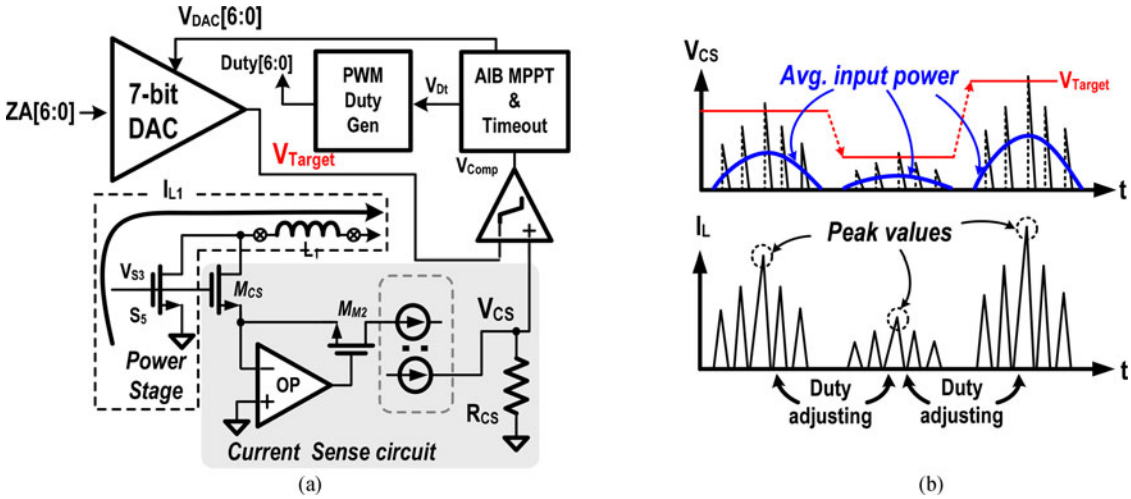


Fig. 17 (a) AIB-MPPT circuit and (b) timing diagram.

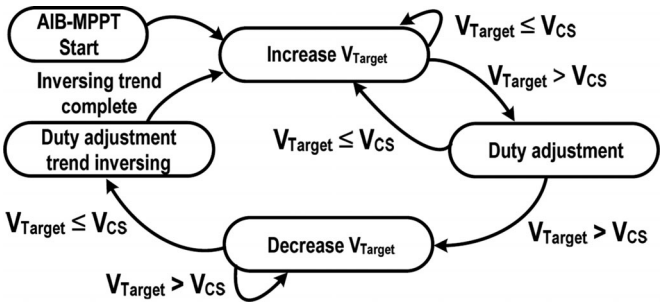


Fig. 18. AIB-MPPT FSM.

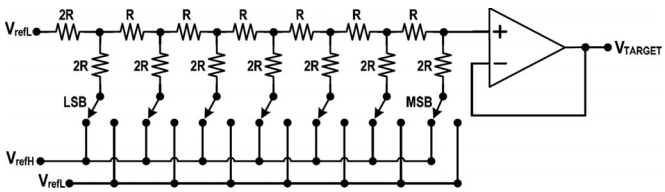


Fig. 19. R-2R DAC.

if the ratio of input voltage to the average input current is considered. This is called the resistance emulation scheme [16], [22]. Equivalent resistance can be determined by calculating the average input current. To illustrate, Fig. 13(a) and (b) shows the charging and discharging phases of the buck–boost converter, respectively, which are derived when a buck–boost converter with a constant switching frequency PWM control operates in DCM. In the DCM operation, inductor current will be released to zero in every clock cycle. Fig. 14 shows the timing diagram of the inductor current when input voltage varies in the situation where the PWM clock and duty are fixed.

The converter's average input current $I_{\text{in},\text{avg}}$ is shown as

$$I_{\text{in,avg}} = \frac{I_{\text{peak}} \cdot D}{2T} = \frac{V_{\text{in}} T \cdot D^2}{2L} \tag{5}$$

where $I_{\text{Peak}}$ is the peak current in the charging phase, $D$ is the duty cycle, $T$ is the time of a switching period, and $L$ is the inductor.

By dividing input voltage $V_{\text{in}}$ by $I_{\text{in,avg}}$, equivalent resistance $R_{\text{eq}}$ can be derived using (6), which is related to $L$, $D$, and $T$

$$R_{\text{eq}} = \frac{V_{\text{in}}}{I_{\text{in,avg}}} = \frac{2L}{TD^2}. \tag{6}$$

Normally, the control factor can be $D$ or $T$ because $L$ is a selected value and cannot be used as a control factor of the equivalent resistance. As shown in Fig. 15(a), duty or switching frequency (controls $T$) can be used to adjust the value of $R_{\text{eq}}$ through PWM or pulse frequency modulation (PFM) control. Thus, the converter can be regarded as a tunable resistance to match the inner impedance and to obtain the maximum output power.

Several considerations in relation to the resistance emulation method should be noted. First, in the selection of converter parameters, $R_{\text{eq}}$ should fit the inner impedance of the harvesting source. The coverage range of $R_{\text{eq}}$ should be designed according to the target source. If a switching converter is used as the emulated resistor, a low-switching frequency will result in a large switching current ripple. If the energy source's driving capability is not sufficient to sink current, the source's terminal will reduce significantly. Large voltage variation on some energy sources, such as a solar cell that has complex equivalent internal models, will influence the output power condition. Even if the equivalent resistance is the ratio of the average input voltage and current, large voltage variation may cause extra power loss or may diverge the power condition from the MPP.

Under the resistor emulation approach, the MPPT controller adjusts the control factor of the resistor emulation converter, such as the duty or the frequency. However, resistor emulation only adjusts the operation point. Adjusting the operation mode changes the emulated loading to match the characteristic of the harvesting source. However, determining the MPP requires the MPPT method. The output power of the energy source should be sampled to define the power status. Based on the power status, the adjustment is meaningful. By continuously sampling and comparing the power status through the adjustment, the harvesting system can eventually operate at the MPP

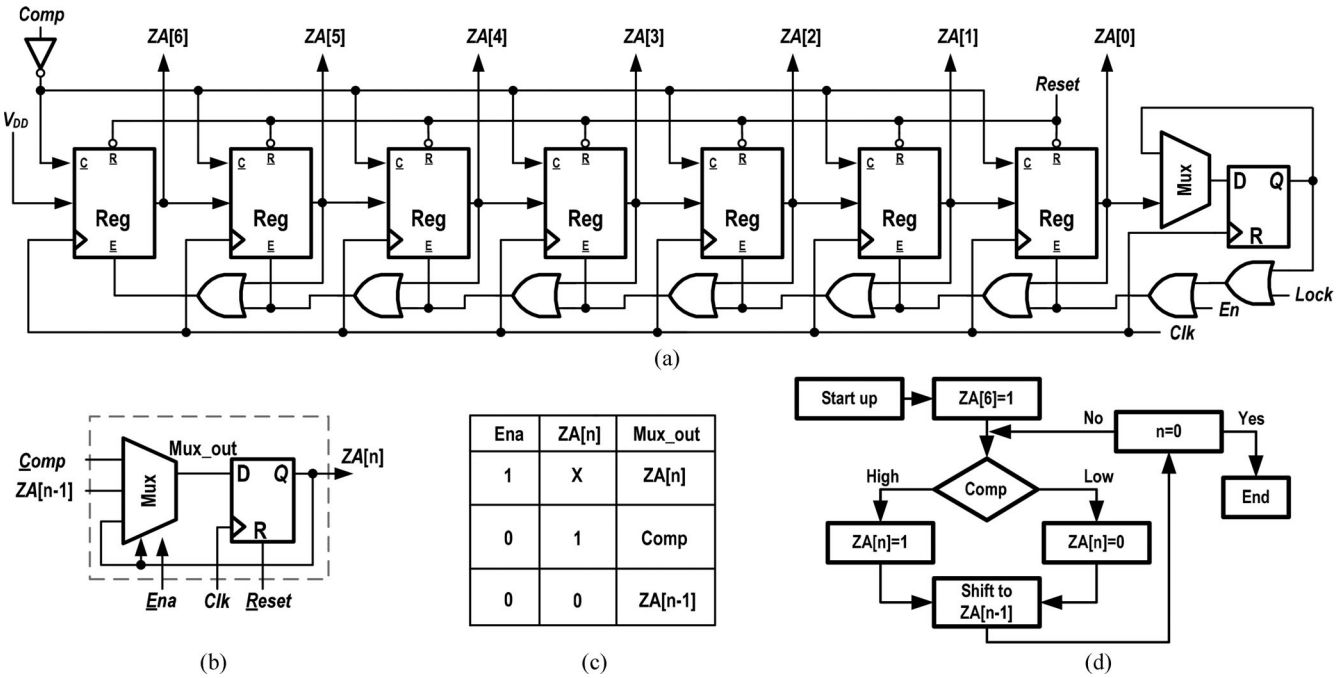


Fig. 20 (a) Seven-bit SAR circuit. (b) Register. (c) Truth table. (d) Flowchart.

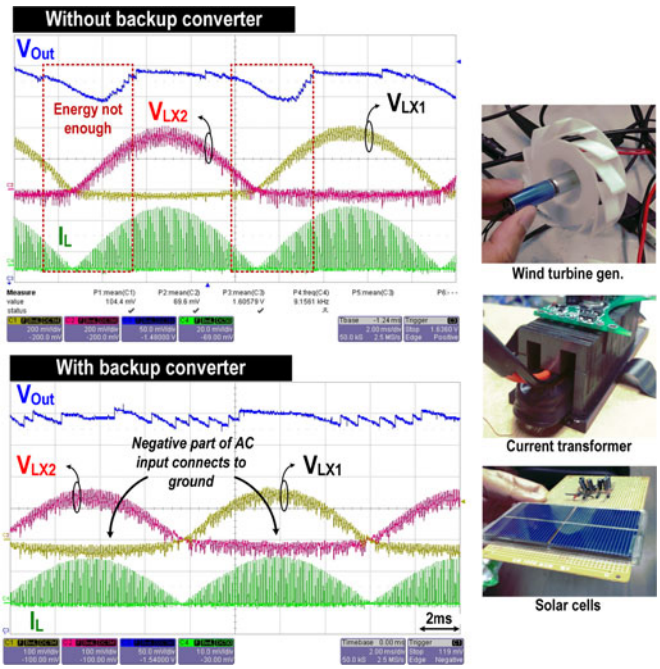


Fig. 21. Measured ac input conversion with and without backup converter.

of the energy source. Different harvesting sources and operation conditions require various tracking methods to obtain MPP.

For harvesting sources with complex models and behaviors, the general way of tracking the MPP is hill climbing, which is also called the P&O method [1], [16]. This method has been used on solar cells for decades because of the complex output power behavior of solar cells under various environmental conditions. To illustrate, output power and output current versus output voltage of a solar cell with the MPPT operation is shown in Fig. 15(b). At the start of adjusting the MPPT process, the output power is measured after each adjustment. If power increases, further adjustment in the same direction is attempted until power increase is prevented. If power decreases, the adjustment changes to the inverse direction. This scheme is similar to the hill-climbing method because it tracks the power curve. Once the adjustment is beyond the MPP, the output power falls below the MPP. The adjustment turns into the inverse direction and traces back to the MPP. The tracking operation goes back and forth around the MPP. To continue tracking the output power, the MPPT keeps on operating to deal with the environmental variations. Thus, if the environmental condition is stable, the adjustment will terminate in a limiting cycle oscillation.

### C. Analog Iterative MPPT

The hill-climbing method compares the power status after each sampling and adjusting. However, this method is not suitable for simultaneous sampling and adjusting of ac or dc sources. The iterative-based MPPT method diverts the comparison issue from the previous sampled power status to a dynamic target power through the MPPT in the ac or dc source. First, the target power is allowed to trace the present sampled power status. Next, the target power level is promoted and the converter is adjusted to enable the output power to reach the target. The procedure is repeated, and the power target and sampled power status iteratively track each other to reach the MPP.

Fig. 16 shows the tracking operation. A target power represented by voltage signal $V_{\rm Target}$ is compared with the peak of the current sense signal $V_{\rm CS}$. At the beginning, $V_{\rm Target}$ is set to be higher than $V_{\rm CS}$. A timeout period $T_O$ is designed as the settling time for the converter and the energy harvesting source. If $V_{\rm Target}$ and $V_{\rm CS}$ do not encounter each other within the

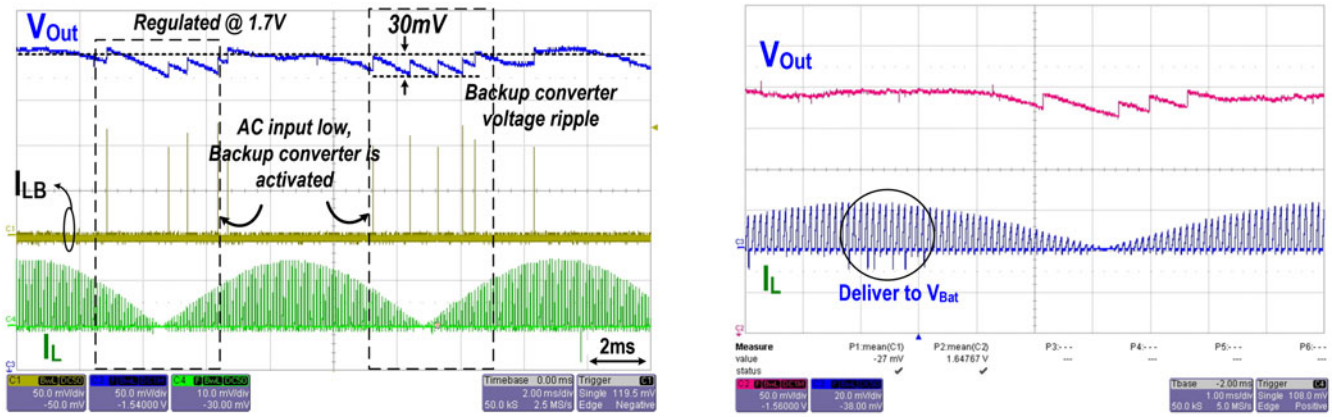


Fig. 22. Measured (a) $I_{\mathrm{LB}}$ and (b) $I_L$ of ac input conversion.

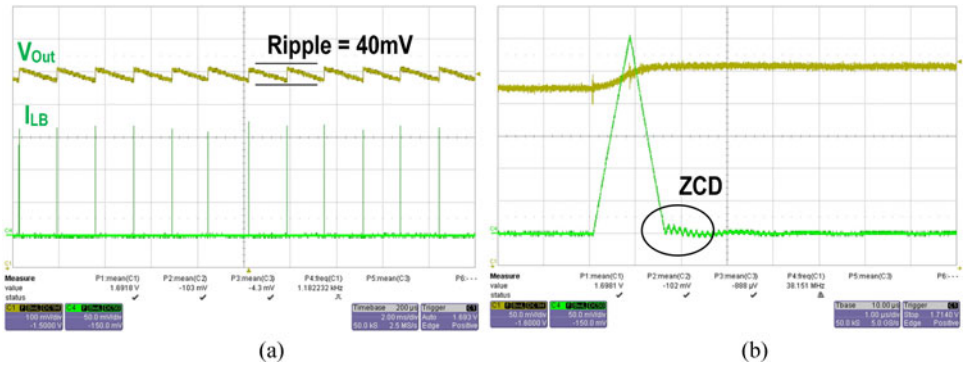


Fig. 23. Output ripple and ZCD of the backup converter.

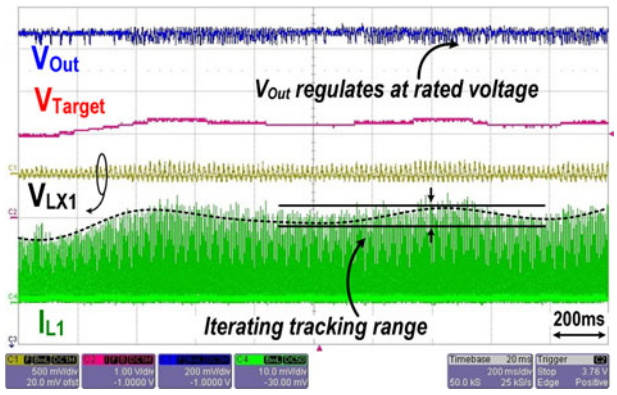


Fig. 24. Measured AIB-MPPT tracking.

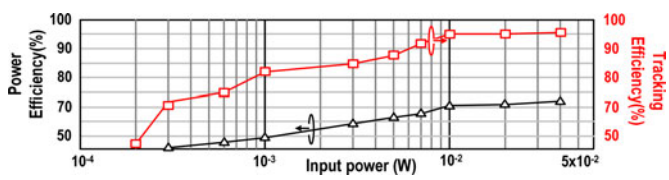


Fig. 25. Measured power and tracking efficiency.

timeout period, $V_{\mathrm{Target}}$ will be set to a lower level. Through several comparisons, $V_{\mathrm{Target}}$ will approach $V_{\mathrm{CS}}$. Moreover, $V_{\mathrm{Target}}$ represents the recent power status. $V_{\mathrm{Target}}$ is set to a slightly higher level as a new target for $V_{\mathrm{CS}}$. The MPPT controller adjusts the PWM duty and checks the variation of $V_{\mathrm{CS}}$. The adjustment may cause output power fluctuation. The increase of $V_{\mathrm{CS}}$ to $V_{\mathrm{Target}}$ before the timeout indicates that output power rises and the duty adjusting trend is correct. Subsequently, $V_{\mathrm{Target}}$ shifts to a higher level as the new target. The adjusting trend continues at the same direction. However, if $V_{\mathrm{CS}}$ cannot reach $V_{\mathrm{Target}}$, an incorrect adjustment trend occurs. After the timeout, the MPPT controller lowers $V_{\mathrm{Target}}$ to determine $V_{\mathrm{CS}}$ and to change the adjusting trend. In conclusion, $V_{\mathrm{Target}}$ is always set to a slightly higher target value than the recent input power condition.

The inductor peak current is proportional to the average input power because of the characteristics of the fixed-frequency DCM and buck–boost operation. Based on this information for the MPPT, the current sense circuit as shown in Fig. 17(a) is proposed to monitor the input power. Using ac input as an example, Fig. 17(b) shows the signal timing diagram. The digital-to-analog converter (DAC) generates tunable reference $V_{\mathrm{Target}}$ for comparison with current sense voltage $V_{\mathrm{CS}}$ and to determine the inductor peak current. The period of the input source

TABLE I
MEASUREMENT COMPARISONS OF PRIOR HARVESTING SYSTEM

| | ISSCC 2013 [3] | ISSCC 2012 [4] | ISSCC 2012 [6] | This Work |
|---|---|---|---|---|
| Technology | 0.25 $\mu$m | 0.13 $\mu$m | 0.35 $\mu$m | 0.15 $\mu$m |
| Energy source | PZT | Thermal | Solar | Magnetic, solar, wind, PZT |
| Input type | AC | DC | DC | AC or DC |
| Rectifier | Full bridge | N/A | N/A | Direct AC/DC |
| Converter type | Buck | Boost | Boost | Buck-Boost |
| Storage | Li-ion battery | N/A | N/A | Li-ion battery |
| MPPT algorithm | VS-P&O | Open circuit P&O | P&O | AIB-MPPT |
| Regulated output | No | Yes | No | Yes |
| Input power | 25 $\mu$W–1.6 mW | 40 | 2.25 W $-$ 36 W | 200 $\mu$W $-$ 50 mW |
| Input voltage | 5–60 V | 40 mV to 0.3V | $<$4.5 V | 0.06–5 V |
| Output voltage | 2–5 V | 2 V | 12 V | Regulated: 1.2–2.5 V Charge: 2.6–4.2 V |
| Controller Power | N/A | N/A | 3.68 mW | 35 $\mu$W |
| Efficiency | $88.7\%@V_{\rm IN} = 30$ V | $61\%@V_{\rm IN} = 0.3$ V | N/A | $72.5\%@V_{\rm IN} = 3$ V Solar |
| Die size | 9.52 mm$^2$ | 0.09 mm$^2$ | 0.441 mm$^2$ | 1.69 mm$^2$ |

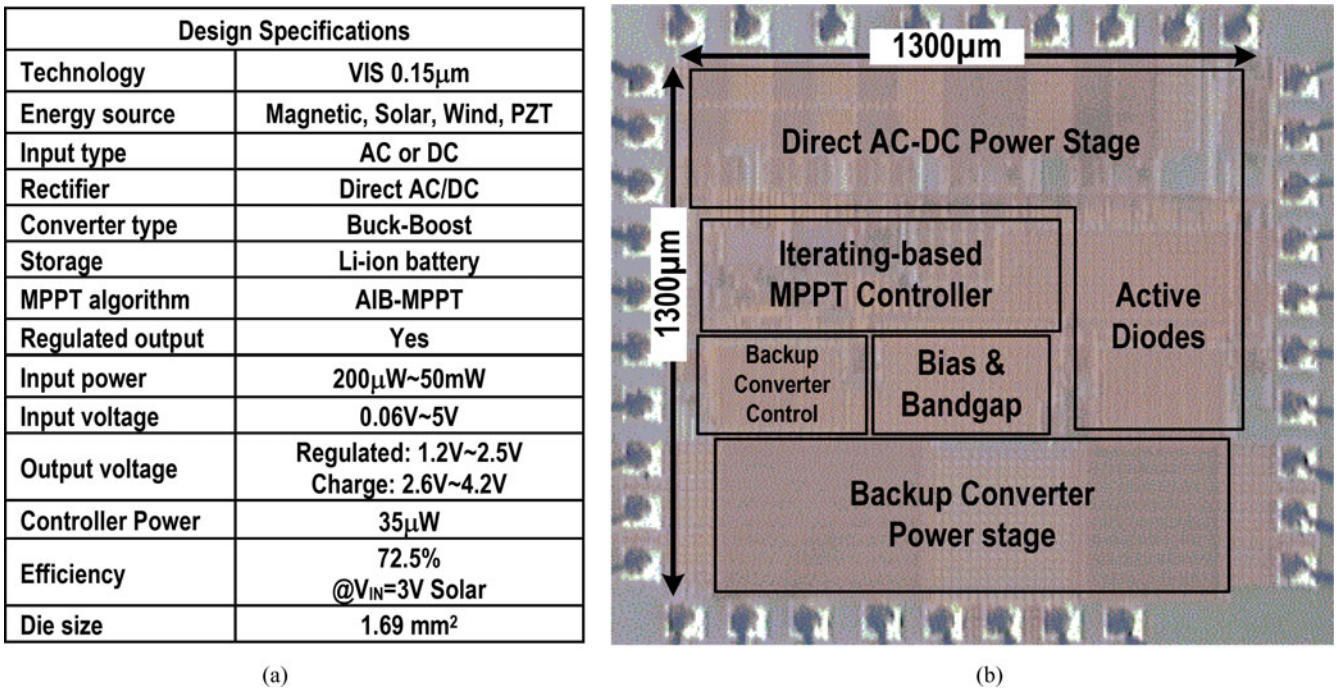


Fig. 26 (a) Design specifications. (b) Chip micrograph.

is unknown; thus, the timeout circuit can determine the comparison sampling timing. Fig. 18 shows the AIB-MPPT finite-state machine (FSM). During AIB-MPPT tracking, $V_{\rm Target}$ is supposed to be higher than $V_{\rm CS}$, and the AIB-MPPT sets $V_{\rm Target}$ to a lower level because comparator output $V_{\rm Comp}$ is not triggered to a height within 200 ms. Through several comparisons, $V_{\rm Target}$ reaches $V_{\rm CS}$ to represent the recent input power level. $V_{\rm Target}$ is set to a slightly higher level as the new target for $V_{\rm CS}$. The AIB-MPPT adjusts the PWM duty and checks the variation of $V_{\rm CS}$. The adjustment may cause output power fluctuation. The increase of $V_{\rm CS}$ to $V_{\rm Target}$ before the timeout indicates that output power rises and the duty adjusting trend is correct. $V_{\rm Target}$ shifts to a higher level as the new target. The adjusting trend continues in the same direction. However, if $V_{\rm CS}$ cannot reach $V_{\rm Target}$, an incorrect adjusting trend occurs. After the timeout, the AIB-MPPT lowers $V_{\rm Target}$ to determine $V_{\rm CS}$ and to change the adjusting trend. In conclusion, $V_{\rm Target}$ should always be set to be a slightly higher target than the recent input power condition. After repeating the procedure, $V_{\rm Target}$ and $V_{\rm CS}$ will iteratively track each other to attain MPP [5].

The sensing information will be converted by one R-2R DAC circuit (Fig. 19) and one 7-bit successive approximation register (SAR) to form the binary search shown in Fig. 20(a). The 7-bit SAR circuit is composed of five registers, a multiplexer (MUX), and a D flip-flop (DFF). The register in Fig. 20(b) operates through the truth table in Fig. 20(c). Ena denotes the enable signal. The overall operation is expressed in the flowchart shown in Fig. 20(d). After each comparison, the current working register will trigger the next register to set the control code ZA[$n - 1$] $= 1$ for the sequent comparison and will subsequently

receive the comparison result from the Comp to adjust output ZA[$n$] to 1 or 0.

After the seven-cycle comparison, the least significant bit is determined, and the last DFF increases and locks out. The output of the 7-bit SAR will be used to derive the accurate off-time value. An additional signal "Lock" derived from the off-chip control can lock out the 7-bit SAR or allow the LSB of the 7-bit SAR to work continuously. When the calibration is completed, the AIB-MPPT circuit is shut down to save power. The tuning range of the sensing circuit has an input voltage tolerance from 1.2 to 2.5 V. The current mismatch can achieve 110% at the input voltage of 1.5 V.

## IV. Experimental Results

The proposed CSE harvesting circuit is tested using four input sources: wind turbine generator, current transformer (CT), solar cells, and piezoelectric transducer (PZT) [23]. The measured ac input conversion with and without the backup converter is shown in Fig. 21. Measurement results indicate that the CSE harvesting circuit rectifies the ac input current and directly supplies $V_{\rm Out}$. The CSE selects a negative terminal from the ac source and connects the negative terminal to the harvesting circuit's ground automatically. Thus, the circuit does not experience a voltage lower than that of the ground. $V_{\rm Out}$ drops periodically because of the energy dead band in the ac source. During this process, the system can be supplied by the backup converter to obtain extra energy and to ensure high-quality and regulated voltage. The voltage ripple can be less than 30 mV, as shown in Fig. 22(a). By contrast, Fig. 21 shows the conversion without the backup converter. The waveform has a significant voltage drop at $V_{\rm Out}$ during the trough of ac waveforms. When the energy delivered to $V_{\rm Out}$ is sufficient, the extra energy will be used to charge the battery. The slope of $I_L$ is significantly steeper when energy is delivered to the battery, as indicated in Fig. 22(b). Fig. 23 shows the output ripple and ZCD waveforms of the backup converter. Fig. 24 shows that the AIB-MPPT can track the maximum input power and damp within a small range. The CSE system reaches a peak power efficiency of 72.5% and tracking efficiency of 94.6%, as shown in Fig. 25. Maximum power efficiency can be calculated based on Eqs. (1) and (4). Tracking efficiency is based on (3) and (6). Table I shows a comparison with the findings of previous studies [3], [4], [6]. The proposed work harvests energy from either ac or dc sources. Input voltage range is not limited by output voltage because of the buck–boost structure. By eliminating the complex data processing, the proposed AIB-MPPT achieves direct ac source MPPT as well as the benefit of area and energy efficiency. Fig. 26 shows the design specifications and chip micrograph with an active area of 1.69 mm$^2$ in VIS 0.15 $\mu$m BCD process [5].

## V. Conclusion

Most state-of-the-art harvesting circuits can only receive dc energy source or single frequency ac energy source. Moreover, harvesting ac source energy requires a diode bridge rectifier, which leads to more power losses. A direct AC–DC and DC–DC CSE harvesting circuit with AIB MPPT technique is proposed in this paper. The buck–boost conversion of CSE automatically converts ac or dc input into dc output without being limited by the universal input voltage range. In AC–DC conversion, the CSE harvesting circuit can accept wide range of ac sources including the non-periodic ac source through the use of the AIB-MPPT technique. Furthermore, the proposed AIB-MPPT technique achieves 94.6% tracking efficiency without complex data calculation and storage that have not been achieved by previous techniques. A backup converter connecting $V_{\rm Bat}$ and $V_{\rm Out}$ is designed to guarantee output voltage stability.

## References


[1] Y.-K. Tan and S. K. Panda, "Optimized wind energy harvesting system using resistance emulator and active rectifier for wireless sensor nodes," *IEEE Trans. Power Electron.*, vol. 26, no. 1, pp. 38–50, Jan. 2011.

[2] K. Kadirvel, Y. Ramadass, U. Lyles, J. Carpenter, V. Ivanov, V. McNeil, A. Chandrakasan, and B. Lum-Shue-Chan, "A 330 nA energy-harvesting charger with battery management for solar and thermoelectric energy harvesting," in *Proc. ISSCC Dig. Tech. Papers*, Feb. 2013, pp. 106–108.

[3] S. Stanzione, C. Van Liempd, R. Van Schaijk, Y. Naito, R. F. Yazicioglu, and C. Van Hoof, "A self-biased 5-to-60V input voltage and 25-to-1600 $\mu$W integrated DC–DC buck converter with fully analog MPPT algorithm reaching up to 88% end-to-end efficiency," in *Proc. ISSCC Dig. Tech. Papers*, Feb. 2013, pp. 74–75.

[4] J.-P. Im, S.-W. Wang, K.-H. Lee, Y.-J. Woo, Y.-S. Yuk, T.-H. Kong, and S.-W. Hong, "A 40 mV transformer-reuse self-startup boost converter with MPPT control for thermoelectric energy harvesting," in *Proc. ISSCC Dig. Tech. Papers*, Feb. 2012, pp. 104–106.

[5] T.-C. Huang, M.-J. Du, K.-L. Lin, S. S. Ng, K.-H. Chen, and C.-L. Wey, "A direct AC–DC and DC–DC cross-source energy harvesting circuit with analog iterating-based MPPT technique with 72.5% conversion efficiency and 94.6%," in *Proc. Symp. VLSI Circuits Dig. Tech. Papers*, 2014, pp. 1–2.

[6] R. Enne, M. Nikolic, and H. Zimmermann, "A maximum power-point tracker without digital signal processing in 0.35$\mu$m CMOS for automotive applications," in *Proc. ISSCC Dig. Tech. Papers*, Feb. 2012, pp. 102–104.

[7] S. Priya and D. J. Inman, *Energy Harvesting Technologies*. New York, NY, USA: Springer, 2009.

[8] Y. Yang, F. Lambert, and D. Divan, "A survey on technologies for implementing sensor networks for power delivery systems," in *Proc. IEEE Power Eng. Soc. Gen. Meeting*, Jun. 2007, pp. 1–8.

[9] S. J. Roundy, "Energy scavenging for wireless sensor nodes with a focus on vibration to electricity conversion," Ph.D. dissertation, Engineering-Mechanical Engineering, University of California, Berkeley, USA, 2003.

[10] J. A. Paradiso and T. Starner, "Energy scavenging for mobile and wireless electronics," *IEEE Pervasive Comput.*, vol. 4, no. 1, pp. 18–27, Jan. 2005.

[11] L. Mateu and F. Moll, "Review of energy harvesting techniques and applications for microelectronics," in *Proc. SPIE*, 2005, vol. 5837, pp. 359–373.

[12] Y. K. Ramadass and A. P. Chandrakasan, "A battery-less thermoelectric energy harvesting interface circuit with 35 mv startup voltage," *IEEE J. Solid-State Circuits*, vol. 46, no. 1, pp. 333–341, Jan. 2011.

[13] E. J. Carlson, K. Strunz, and B. P. Otis, "A 20 mV input boost converter with efficient digital control for thermoelectric energy harvesting," *IEEE J. Solid-State Circuits*, vol. 45, no. 4, pp. 741–750, Apr. 2009.

[14] *Thermoelectric generators* [Online]. Available: http://www.tellurex.com/

[15] N. Elvin and A. Erturk, *Advances in Energy Harvesting Methods*. New York, NY, USA: Springer, 2013.

[16] S. Bandyopadhyay and A. P. Chandrakasan, "Platform architecture for solar, thermal, and vibration energy combining with MPPT and single inductor," *IEEE J. Solid-State Circuits*, vol. 47, no. 9, pp. 2199–2215, Sep. 2012.

[17] E. Koutroulis and K. Kalaitzakis, "Design of a maximum power tracking system for wind-energy-conversion applications," *IEEE Trans. Ind. Electron.*, vol. 53, no. 2, pp. 486–494, Apr. 2006.

[18] Y.-K. Tan and S. K. Panda, "Self-autonomous wireless sensor nodes with wind energy harvesting for remote sensing of wind-driven wildfire spread," *IEEE Trans. Power Electron.*, vol. 26, no. 4, pp. 1367–1377, Apr. 2011.

[19] T. Paing, E. Falkenstein, R. Zane, and Z. Popovic, "Custom IC for ultra-low power RF energy harvesting," *IEEE Appl. Power Electron. Conf. Expo.*, 2009, pp. 1239–1245.

[20] D. Kwon and G. A. Rincon-Mora, "A single-inductor AC–DC piezoelectric energy-harvester/battery-charger IC converting ± (0.35 to 1.2V) to (2.7 to 4.5V)," in *Proc. ISSCC Dig. Tech. Papers*, Feb. 2010, pp. 494–495.
[21] T.-C. Huang, M.-J. Du, Y.-Y. Yang, Y.-H. Lee, Y.-C. Kang, R.-H. Peng, and K.-H. Chen, "Non-invasion power monitoring with 120% harvesting energy improvement by maximum power extracting control for high sustainability power meter system," in *Proc. IEEE Custom Integr. Circuits Conf.*, Sep. 2012, pp. 1–4.
[22] T. Paing, J. Shin, R. Zane, and Z. Popovic, "Resistor emulation approach to low-power RF energy harvesting," *IEEE Trans. Power Electron.*, vol. 23, no. 3, pp. 1494–1501, May 2008.
[23] Midé Technology Corporation, V25W-ND, Piezoelectric energy harvesters, Jan. 2013.

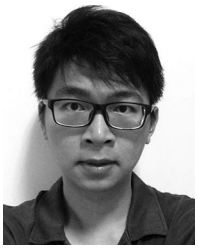

**Shin-Hao Chen** was born in Taichung, Taiwan. He received the B.S. degree in electronic engineering from National Tsing Hua University, Hsinchu, Taiwan, in 2010, and the M.S. degree in 2012 in display technology from National Chiao Tung University, Hsinchu. He is currently working toward the Ph. D. degree at the Institute of Electrical Engineering.

He is a Member of the Mixed-Signal and Power Management IC Laboratory, National Chiao Tung University. He is currently involved in working on class-D amplifiers and power management circuit design. His current research interests include the power management IC design, analog integrated circuits, and mixed signal IC design.

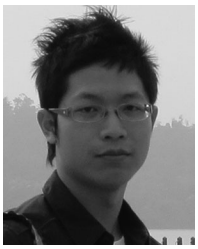

**Tzu-Chi Huang** was born in Hsinchu, Taiwan, 1983. He received the B.S. and M.S. degrees from the Department of Electrical Engineering, National Cheng Kung University, Tainan, Taiwan, and the Ph.D. degree from the Institute of Electrical Control Engineering, National Chiao Tung University, Hsinchu, Taiwan, in 2014.

His current research interests include the power management IC design, analog integrated circuits, and mixed signal IC design. He is currently a Design Engineer at MediaTek Inc., Hsinchu, Taiwan.

**Shao Siang Ng** was born in Johor Bahru, Johor, Malaysia. He received the B.S. degree from the Department of Electrical Engineering, National Chi Nan University, Nantou, Taiwan, in 2011, and the M.S. degree from the Department of Electrical Engineering, National Chiao Tung University, Hsinchu, Taiwan, in 2013.

He is a Member of the Mixed Signal and Power Management IC Laboratory, National Chiao Tung University. He is currently a Design Engineer at MediaTek Inc., Hsinchu, Taiwan. His current research interests include the design of integrated power management IC design and class-D audio amplifier.

**Kuei-Liang Lin** was born in Yilan, Taiwan, in 1989. He received the B.S. and M.S. degrees from the Department of Electrical and Computer Engineering, National Chiao Tung University, Hsinchu, Taiwan, in 2012 and 2014, respectively.

He is a Member of the Mixed Signal and Power IC Laboratory, Institute of Electrical Control Engineering, National Chiao Tung University. His current research interests include power management IC and analog IC design.

**Ming-Jhe Du** was born in Tainan, Taiwan, in 1981. He received the B.S. degree in electrical engineering from National Cheng Kung University (NCKU), Tainan, Taiwan, in 2003, and the M.S. degree in electrical engineering from National Taiwan University (NTU), Taipei City, Taiwan, in 2006.

**Yu-Chai Kang** was born in Yilan, Taiwan. He received the B.S. degree from the Department of Electrical Engineering, National Chiao Tung University, Hsinchu, Taiwan, where he is currently working toward the M.S. degree at the Institute of Department Electrical Engineering.

He is a Member of the Mixed-Signal and Power Management IC Laboratory, National Chiao Tung University. Since 2012, he has been an Engineer with Taiwan Semiconductor Manufacturing Corp. (TSMC), Hsinchu. His current research interests include the power management IC design, analog integrated circuits, and mixed signal IC design.

**Ke-Horng Chen** (M'04–SM'09) received the B.S., M.S., and Ph.D. degrees in electrical engineering from National Taiwan University, Taipei, Taiwan, in 1994, 1996, and 2003, respectively.

He is currently a Director and Professor of the Institute of Electrical Control Engineering, National Chiao Tung University, Hsinchu, Taiwan, where he is involved in organizing the Mixed-Signal and Power Management IC Laboratory. He is the author or coauthor of more than 200 papers published in journals and conferences and also holds more than 40 U.S. patents and 40 Taiwan patents. His current research interests include power management ICs, display algorithm and driver designs of liquid crystal display (LCD) TV, wireless power transfer, and energy harvesting circuit designs.

Dr. Chen was an Associate Editor of the IEEE TRANSACTIONS ON POWER ELECTRONICS, the IEEE TRANSACTIONS ON CIRCUITS AND SYSTEMS—PART I: REGULAR PAPERS, and the IEEE TRANSACTIONS ON CIRCUITS AND SYSTEMS—PART II: EXPRESS BRIEFS. He is the CAS Taipei Section Chair from 2015. He is the Technical Program Committee Member, European Solid-State Circuits Conference (ESSCIRC) (2014–present). He is a member of the IEEE Circuits and Systems (CAS) VLSI Systems and Applications Technical Committee and the IEEE CAS Power and Energy Circuits and Systems Technical Committee.

**Chin-Long Wey** (M'83–SM'97–F'11) received the Ph.D. degree in electrical engineering from Texas Tech University, Lubbock, USA, in 1983.

He is currently the University Distinguished Professor of Electrical Engineering at National Chiao Tung University (NCTU), Hsinchu, Taiwan. He was the Director General of the National Chip Implementation Center (CIC), Hsinchu, Taiwan, in 2007–2010, and the Dean of College of Electrical Engineering and Computer Science at National Central University (NCU) in 2003–2006. He came to NCU from Michigan State University where he was a tenured full professor of Electrical and Computer Engineering Department from 1983 to 2003 for 20 years. In 2001, he started up a Fab-less design house, JMicron Technology Corp, in Hsinchu Science-based Park, Taiwan, that develops and markets high-speed serial link products. His research interests include design, testing, and fault diagnosis of analog/mixed-signal VLSI circuits and systems; Power electronics; Power management systems; and Smart battery management systems. Dr. Wey is a Fellow of the IEEE.

**Ying-Hsi Lin** received the B.S. degree from National Chiao-Tung University, Hsinchu, Taiwan, in 1993, and the M.S. degree in electrical engineering from National Taiwan University, Taipei, Taiwan, in 1995.

He joined Computer and Communication Research Lab, ITRI, as a Researcher in 1995, and became the Project Leader of CMOS RF and high-speed mixed-signal circuits design in 1998. He was involved in CMOS radio-frequency-integrated circuits and mixed-signal circuits IC design for computer and communication application. In October 1999, he joined Realtek Semiconductor Corp., as a RF manager, where he was responsible for several R&D CMOS RF projects including Bluetooth, WLAN 802.11abg, 802.11n, WLAN CE and UWB, and also involving CMOS RF IC mass production planning. In the circuits design, he is involved in designing RF synthesizer, LNA, mixer, modulator, PA, filter, PGA, mixed-signal circuits, ESD circuits, RF device modeling, RF system calibration, and communication system design. In 2010, he became the Vice President and led the Research and Design Center of Realtek. He holds more than 30 patents in the area of mixed-signal and RF IC design.

**Chao-Cheng Lee** received the B.S. degree in electrical engineering from National Chiao Tung University, Hsinchu, Taiwan, in 1988, and the M.S. degree in physics from National Taiwan University, Taipei, Taiwan, in 1990.

He joined Realtek Semiconductor, Hsinchu, Taiwan, in 1992, where he is currently the Senior Vice President of Engineering. His current research interests include phase-locked loops, filters, high-speed OP, and mismatch calibration. He has more than 30 U.S. patents granted or pending.

**Jian-Ru Lin** was born in Nantou, Taiwan, in 1978. He received the B.S. degree in electronic engineering from National Taiwan University of Science and Technology, Taipei, Taiwan, in 2000, and the M.S. degree in electronic engineering from National Taiwan University, Taipei, in 2003.

In 2003, he joined the R&D Center, Realtek Semiconductor Corp., Hsinchu, Taiwan, where he is currently the Director. His current research interests include analog and mixed-mode circuit design, high-speed/resolution data converters, and timing recovery for communications, high-efficiency line driver, and power management IC.

**Tsung-Yen Tsai** was born in Pingtung, Taiwan. He received the B.S. degree from National Sun Yat-Sen University, Kaohsiung, Taiwan, in 2004, and the M.S. degree in communication engineering from National Chiao Tung University, Hsinchu, Taiwan, in 2006.

He joined Realtek Semiconductor Corporation, Hsinchu, Taiwan, in July 2006, as an Analog Circuit Designer. He is currently involved in GPS, Bluetooth, WLAN802.11abg, 802.11n, and 802.11ac. His current research interests include current DAC and switching regulators for SoC.